length l, or $P_{th} = P_s(l) = P_p(l) = P_0 \exp(-\alpha l)$, where $P_0 = I_p(0)A_{eff}$. Following the approaches taken by Smith (eqns. 9 and 17 in Reference 1), at the threshold we have

$$\frac{\sqrt{(\pi)}}{2}\left(\frac{f_s}{f_a}\right)KT\left(\frac{A_{eff}}{g_B P_{th} L_{eff}}\right)^{1/2} \Delta f G\bigg|_{P_0 = P_{th}} = P_{th}\left(\frac{P_{th} g_B L_{eff}}{A_{eff}}\right) \tag{9}$$

In eqn. 9 the Brillouin gain is assumed to have a Lorentzian spectral profile and g_B is the peak gain. Δf is the spectral width of the Brillouin-gain spectrum.[12] K is Boltzmann's constant. T is the temperature and f_a is frequency of the acoustic phonon.[1,6] Substituting eqns. 6–8 into 9 we can have

$$\begin{aligned}\frac{\sqrt{(\pi)}}{2}\left(\frac{f_s}{f_a}\right)KT\left(\frac{g_B L_{eff}}{A_{eff}}\right)\Delta f &= \left(\frac{P_{th} g_B L_{eff}}{A_{eff}}\right)^{5/2} \\ &\times \exp\left(-\frac{P_{th} g_B L_{eff}}{A_{eff}}\right)\left\{1 + \frac{2\kappa A_{eff}\exp(\alpha L/2)}{g P_{th}}\left[\frac{I_p(0)}{I_s(L)}\right]^{1/2} \right. \\ &\left. \times \left[1 - \exp\left(\frac{-g P_{th} L_{eff}}{2A_{eff}}\right)\right]\right\}^{-2}\end{aligned} \tag{10}$$

If $\kappa = 0$, then $\eta = 0$ and eqn. 10 reduces to a previously reported relation (eqn. 17 in Reference 1). Using the same data given in Reference 1 and 12, eqn. 10 is evaluated. Fig. 2 shows the value of P_{th} as a function of κL with $\sqrt{[I_s(L)/I_p(0)]} = 0.001$. This figure indicates that increasing Bragg diffraction decreases P_{th}. It is noted that the parameter $\sqrt{[I_s(L)/I_p(0)]} = 0.001$ is arbitrarily chosen but Agrawal has used this value in Reference 12.

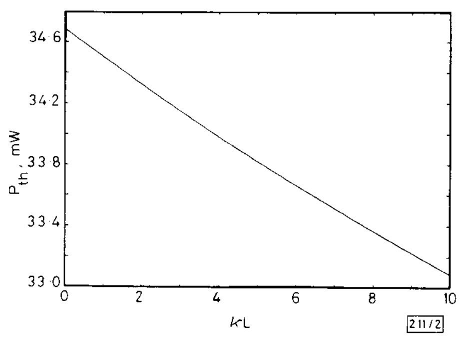

Fig. 2 *Effect of Bragg diffraction (κL) on the threshold P_{th} of SBBS with $\sqrt{[I_s(L)/I_p(0)]} = 0.001$*

Conclusions: A perturbation analysis including the nonlinear interaction between the pump and Stokes waves, optical loss and Bragg diffraction of stimulated backward Brillouin scattering (SBBS) in single mode optical fibres has been presented. We have found that a larger Bragg diffraction induces a higher Brillouin gain. The relation between the threshold of SBBS and the Bragg diffraction is reported for the first time. Furthermore, increasing Bragg diffraction decreases the threshold of the SBBS. Because Bragg diffraction is an acousto-optic interaction phenomenon the acoustic guidance conditions in the singlemode optical fibre can be used to adjust the Brillouin gain and the threshold.[1]

Acknowledgment: C. A. S. de Oliveira would like to thank FAPESP (Fundacao de Amparo a Pesquisa do Estado de Sao Paulo) for a fellowship.

C. A. S. DE OLIVEIRA*
C. K. JEN
IMI
National Research Council
Boucherville, Quebec, Canada J4B 6Y4

18th February 1991

* On leave of absence from Escola Politecnica da Universidade de Sao Paulo, Sao Paulo, Brazil

References

1 SMITH, R. G.: 'Optical power handling capacity of low loss optical fibers as determined by stimulated Raman and Brillouin scattering', *Appl. Opt.*, 1972, **11**, pp. 2489–2494
2 COTTER, D.: 'Stimulated Brillouin scattering in monomode optical fibers', *J. Opt. Comm.*, 1980, **1**, pp. 10–19
3 HORIGUCHI, T., KURASHIMA, T., and TATEDA, M.: 'A technique to measure distributed strain in optical fibers', *IEEE Photonics Technol. Lett.*, 1990, **2**, pp. 352–354
4 KURASHIMA, T., HORIGUCHI, T., and TATEDA, M.: 'Distributed temperature sensing using stimulated Brillouin scattering in optical silica fibers', *Opt. Lett.*, 1990, **15**, pp. 1038–1040
5 STOKES, L. F., CHODOROW, M., and SHAW, H. J.: 'All-fiber stimulated Brillouin ring laser with submilliwatt pump threshold', *Opt. Lett.*, 1989, **7**, pp. 509–511
6 TANG, C. L.: 'Saturation and spectral characteristics of the Stokes emission in the stimulated Brillouin process', *J. Appl. Phys.*, 1966, **37**, pp. 2945–2955
7 ENNS, R. H., and BATRA, I. P.: 'Saturation and depletion in stimulated light scattering', *Phys. Lett.*, 1969, **28A**, pp. 591–592
8 YEH, P., and GU, X. G.: 'Stimulated Brillouin scattering revisited'. Digest of Nonlinear Optics: Materials, Phenomena and Devices Conference, Kauai, Hawaii, July 1990, pp. 141–142
9 THOMAS, P. J., ROWELL, N. L., VAN DRIEL, H. M., and STEGEMAN, G. I.: 'Normal acoustic modes and Brillouin scattering in single mode optical fibers', *Phys. Rev. B*, 1979, **19**, p. 1167
10 SHIBATA, N., OKAMOTO, K., and AZUMA, Y.: 'Longitudinal acoustic modes and Brillouin-gain spectra for GeO_2 doped core single mode fibers', *J. Opt. Soc. Am. B*, 1989, **6**, pp. 1167–1174
11 JEN, C. K., and GOTO, N.: 'Backward collinear guided-wave-acousto-optic interactions in single mode fibers', *J. Lightwave Technol.*, 1989, **7**, pp. 2018–2023
12 AGRAWAL, G. P.: 'Nonlinear fiber optics' (Academic Press, New York, 1989), Chap. 9, pp. 263–288

HEXAGONAL DISCRETE COSINE TRANSFORM FOR IMAGE CODING

Indexing terms: Transforms, Fourier transforms, Image processing

The discrete cosine transform plays an important role in rectangularly sampled image coding for its excellent performance in information compaction. Hexagonal sampling is the optimal sampling strategy for two-dimensional signals in the sense that exact reconstruction of the waveform requires a lower sampling density than with the alternative schemes. In this Letter, a hexagonal discrete cosine transform (HDCT) for encoding the hexagonally sampled signals is presented.

Introduction: The discrete cosine transform can be used in the area of digital processing for the purpose of source encoding.[1,2] Its performance is relatively close to that of the Karhunen-Loeve transform which is known to be optimal.[3] It is known that the hexagonal sampling is the optimal sampling scheme for two-dimensional signals which are bandlimited over a circular region of the Fourier plane, in the sense that exact reconstruction of the waveform requires a lower sampling density than with alternative schemes.[4,7] For such signals, hexagonal sampling requires 13·4% fewer samples than rectangular sampling. In image coding applications, the coding efficiency can be increased by using the hexagonal sampling scheme. In this Letter, a hexagonal discrete cosine transform which can be used in the applications of image coding is described.

Hexagonal DFT: Let $X_a(\omega_1, \omega_2)$ be the Fourier transform of a bandlimited continuous-time signal $x_a(t_1, t_2)$. The periodically extended Fourier transform of $X_a(\omega_1, \omega_2)$ with the period vectors $\Omega^1 = (\omega^{11}, \omega^{12})$ and $\Omega^2 = (\omega^{21}, \omega^{22})$ is denoted by $\tilde{X}_a(\omega_1, \omega_2)$. The periodic extension $\tilde{X}_a(\omega_1, \omega_2)$ can then be determined by $X_a(\omega_1, \omega_2)$ through the convolution

$$\tilde{X}_a(\omega_1, \omega_2) = X_a(\omega_1, \omega_2) * \sum_{n=-\infty}^{\infty} \sum_{m=-\infty}^{\infty} \times \delta(\omega_1 + i\omega^{11} + j\omega^{21}, \omega_2 + i\omega^{12} + j\omega^{22})$$

The inverse Fourier transform is proportional to

$$X_a(t_1, t_2) \cdot \sum_{n=-\infty}^{\infty} \sum_{m=-\infty}^{\infty} \times \delta(\omega^{11}t_1 + \omega^{12}t_2 - 2i\pi, \omega^{21}t_1 + \omega^{22}t_2 - 2j\pi)$$

Let

$$\Delta_\omega = \begin{vmatrix} \omega^{11} & \omega^{12} \\ \omega^{21} & \omega^{22} \end{vmatrix}$$

where $|\ |$ is the determinant of the array. The discrete signal $x(i, j)$ is the signal $x_a(t_1, t_2)$ sampled periodically at

$$\left(\frac{2\pi}{\Delta_\omega}\begin{vmatrix} i & \omega^{12} \\ j & \omega^{22} \end{vmatrix}, \frac{2\pi}{\Delta_\omega}\begin{vmatrix} \omega^{11} & i \\ \omega^{21} & j \end{vmatrix}\right)$$

A two-dimensional lattice is defined as a set of vectors $\{Y : Y = iT^1 + jT^2\}$, where i and j are integers and T^i, $i = 1, 2$ are the basis vectors for the lattice. Thus, the period vectors of the spatial sampling lattice are

$$T^1 = \frac{2\pi}{\Delta_\omega}(\omega^{22}, -\omega^{21}) \quad \text{and} \quad T^2 = \frac{2\pi}{\Delta_\omega}(\omega^{12}, -\omega^{11})$$

Therefore, the discrete signal

$$x(i, j) = x_a(iT^1 + jT^2)$$

The frequency sampling lattice can also be derived in a similar way. Let $T^1 = (T^{11}, T^{12})$ and $T^2 = (T^{21}, T^{22})$ be the spatial periods whose magnitudes are large enough that the periodic extension is not overlapped in the transform domain. Thus, the basis vectors of the frequency sampling lattice are

$$\frac{2\pi}{\Delta_t}(T^{22}, -T^{21}) \quad \text{and} \quad \frac{2\pi}{\Delta_t}(-T^{12}, T^{11}),$$

where

$$\Delta_t = \begin{vmatrix} T^{11} & T^{12} \\ T^{21} & T^{22} \end{vmatrix}$$

For a finite area sequence with the region of support R_t, the generalised DFT may then be expressed as

$$X(u, v) = \sum_{(i, j) \in R_t} x(i, j) \exp(-j\phi(i, j, u, v))$$

and

$$x(i, j) = \frac{1}{M} \sum_{(u, v) \in R_\omega} X(u, v) \exp[j\phi(i, j, u, v)]$$

where M is the number of samples of the signal array

$$\phi(i, j, u, v) = \frac{4\pi^2}{\Delta_\omega \Delta_t}\left(\begin{vmatrix} i & \omega^{12} \\ j & \omega^{22} \end{vmatrix} \cdot \begin{vmatrix} u & T^{12} \\ v & T^{22} \end{vmatrix} + \begin{vmatrix} \omega^{11} & i \\ \omega^{21} & j \end{vmatrix} \cdot \begin{vmatrix} T^{11} & u \\ T^{21} & v \end{vmatrix}\right)$$

and

$$R_\omega = \left\{(u, v) : -\pi < \frac{2\pi}{\Delta_t}\begin{vmatrix} u & T^{12} \\ v & T^{22} \end{vmatrix} \leq \pi, -\pi < \frac{2\pi}{\Delta_t}\begin{vmatrix} T^{11} & u \\ T^{21} & v \end{vmatrix} \leq \pi\right\}$$

Hexagonal DCT: Let $x(i, j)$ be a hexagonally shaped finite area array with a regularly hexagonal support of R_N shown in Fig. 1.

Let $y(i, j)$ be the two-dimensional signal with a support which is composed of two regularly hexagonal arrays. The relationship between $x(i, j)$ and $y(i, j)$ is as follows:

$$y(i, j) = \begin{cases} x(i, j), & j \geq 0 \\ x(-i + N - 2, -j - 1), & j < 0 \end{cases}$$

The spatial period vectors are $T^1 = [(3N - 1)/2, N - 1]$ and $T^2 = (1, 4N - 2)$. In the transform domain, the frequency period vectors are defined as $\boldsymbol{\Omega}^1 = (2\pi, \pi)$ and $\boldsymbol{\Omega}^2 = (0, 2\pi)$.

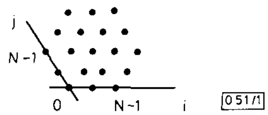

Fig. 1 *Hexagonal array*

$R_N = \{(i, j): 0 < i < 2N - 1, 0 < j < 2N - 1, |i - j| < N\}$

The hexagonal cosine transform becomes

$$X(u, v) = C(u, v) \sum_{(i, j) \in R_N} x(i, j) \cos \psi(i, j, u, v)$$

and the inverse is

$$x(i, j) = \frac{2}{M} \sum_{(u, v) \in R_\omega} C(u, v) X(u, v) \cos \psi(i, j, u, v)$$

where $M = 3N^2 - 3N + 1$ is the number of samples of the signal array

$$C(u, v) = \begin{cases} 1/\sqrt{2}, & \text{for } (u, v) = (0, 0) \\ 1, & \text{elsewhere} \end{cases}$$

$$\psi(i, j, u, v) = \frac{\pi}{3N^2 - 3N + 1}\{(i - N/2 + 1) \times [(4N - 2)u - (N - 1)v] - (j + 0{\cdot}5) \times (2Nu - (2N - 1)v]\}$$

and

$$R_\omega = \left\{\left\{(u, v): -1 < \frac{1}{M}((4N - 2)u - (N - 1)v) < 1, \times 0 < \frac{1}{M}\left(\frac{1}{2}(3N - 1)v - u\right) < 1\right\} \cup \{(u, v): 0 \leq \frac{1}{M}((4N - 2)u - (N - 1)v) < 1, \times \frac{1}{M}\left(\frac{1}{2}(3N - 1)v - u\right) = 0\}\right\}$$

Performance of information compaction: A linear transform can be expressed as

$$X(u, v) = \sum_{(i, j)}\sum x(i, j) \, . \, A(i, j, u, v)$$

The variances of the transform coefficients are

$$E[X(u, v)] = \sum_{(i, j)}\sum \sum_{(k, l)}\sum E[x(i, j)x(k, l)]A(i, j, u, v)A(k, l, u, v)$$

In image processing applications, the Markov process is a useful model for the image data. We discuss the situation where the hexagonal signal meets the first-order Markov model, such as

$$E[x(i, j)x(k, l)] = \rho^{\sqrt{\{[i-k] - (1/2)[j-1]\}^2 + (3/4)[j-1]^2}}$$

The role that orthogonal transforms play in image coding is illustrated in Fig. 2.

The orthogonal transforms compact most of the energy of the signal to a few transform coefficients. Zonal sampling will retain those coefficients whose variances are greater than a given threshold. To demonstrate the energy compaction performance of the proposed hexagonal discrete cosine transform, let the signal be a first-order Markov process with $\rho = 0{\cdot}9$. The transform domain variances of HDCT against HDFT for $N = 3$ are shown in Table 1, in which the variances are placed in decreasing order. We see that the proposed HDCT is more efficient in energy compaction than the HDFT. Therefore, the HDCT is superior to HDFT in image coding applications.

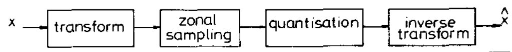

Fig. 2 *Image coding model*

Table 1 TRANSFORM DOMAIN VARIANCES, $\rho = 0.9$, $N = 3$

Component	0	1	2	3	4	5
HDFT variance	15.429	0.386	0.386	0.386	0.386	0.386
HDCT variance	15.429	0.966	0.789	0.215	0.215	0.215

Component	6	7	8	9	10	11	12
HDFT variance	0.386	0.122	0.122	0.122	0.122	0.122	0.122
HDCT variance	0.172	0.135	0.121	0.104	0.101	0.701	0.071

Component	13	14	15	16	17	18
HDFT variance	0.087	0.087	0.087	0.087	0.087	0.087
HDCT variance	0.071	0.069	0.064	0.064	0.064	0.064

Conclusions: A discrete cosine transform for hexagonal arrays is presented. It is shown that the proposed transform is superior to the HDFT in image coding.

H.-S. WU

Institute of Image Processing & Pattern Recognition
Shanghai Jiao Tong University
Shanghai 200030, People's Republic of China

References

1 CLARKE, R. J.' 'Transform coding of images' (Academic Press Inc. 1985).
2 WU, H. S., and CHEN, H. B.: 'A DCT gain-shape vector quantizer for image coding'. ICC'88, Philadelphia, June, 1988
3 AHMED, N., NATARAJAN, T., and RAO, K. R.: 'Discrete cosine transform', *IEEE Trans.*, 1974, **ASSP-22**, pp. 90–93
4 PETERSEN, D. P., and MIDDLETON, D.: 'Sampling and reconstruction of wave-number-limited functions in N-dimensional euclidean spaces', *Inform. Contr.*, 1962, **5**, pp. 279–323
5 MERSEREAU, R. M.: 'The processing of hexagonally sampled two-dimensional signals', *Proc. IEEE*, 1979, **67**, (6), pp. 930–949
6 GUESSOUM, A., and MERSEREAU, R. M.: 'Fast algorithm for the multi-dimensional discrete fourier transform', *IEEE Trans.*, 1986, **ASSP-34**, pp. 937–943
7 MERSEREAU, R. M., and SPEAKE, T. C.: 'The processing of periodically sampled multidimensional signals', *IEEE Trans.*, 1983, **ASSP-31**, pp. 188–194

LINEAR TRANSCONDUCTOR BASED ON CROSSCOUPLED CMOS PAIRS

Indexing terms: Active filters, Circuit theory and design

A circuit technique based on two CMOS crosscoupled pairs for realising a linear CMOS transconductor of class AB is presented. Design tradeoffs are discussed and a circuit example is presented. SPICE simulation results show that, for a power supply of ±5 V, the linearity error is controlled to ±1% over a ±3 V input range.

Introduction: Linear transconductors are useful building blocks in the design of analogue signal processing systems. However, limited linearity is often the major drawback in the use of these circuits in many potential applications. Several attractive approaches for improving the linearity of MOS transconductor circuits have been reported in the literature.[1–6] In Reference 1, a linear transfer characteristic is achieved by two crosscoupled differential pairs operating in saturation. A different technique based on current addition was proposed in Reference 2. Other linearisation methods use additional ideal voltage sources,[3,4] or negative feedback in the form of source-degeneration.[5] Using low-distortion transconductance amplifiers, video frequency continuous-time filters with wide dynamic range are considered in Reference 6.

In this Letter an alternative circuit technique for improving the linearity of a class AB transconductance element is described.

Transconductor cell description: Consider two CMOS pairs (M1, M2) and (M3, M4) in the crosscoupled configuration shown in Fig. 1. Note that the transistors M5 and M6 work as

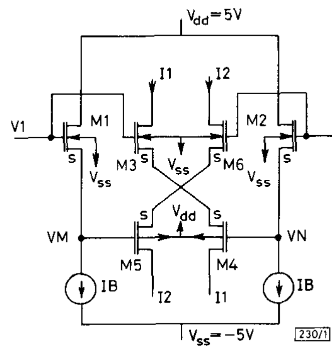

Fig. 1 *Linear CMOS transconductor circuit*

source-followers biased by the DC currents I_B. Using the standard square-law model for MOS devices in their saturation region, the currents I_1 and I_2, defined in Fig. 1, are

$$I_1 = k_{eff}(V_1 - V_N - V_{T\Sigma})^2 \tag{1a}$$

$$I_2 = k_{eff}(V_2 - V_M - V_{T\Sigma})^2 \tag{1b}$$

where

$$k_{eff} = \frac{k_n k_p}{[\sqrt{(k_n)} + \sqrt{(k_p)}]^2} \tag{2}$$

and

$$V_{T\Sigma} = V_{Tn} + V_{Tp} \tag{3}$$

All undefined parameters have their usual meaning. If the transistors M1–M6 operate in saturation, the following equations can be written:

$$V_1 - V_2 = V_M - V_N = V_d \tag{4}$$

$$V_1 - V_M = V_2 - V_N = V_B \tag{5}$$

where $V_d = V_1 - V_2$ is the differential input voltage, and V_B is defined as

$$V_B = \sqrt{(I_B/k_n)} + V_{Tn} \tag{6}$$

With eqns. 4 and 5, the currents I_1 and I_2 can be expressed in terms of the voltage V_B as

$$I_1 = k_{eff}(V_d + V_B - V_{T\Sigma})^2 \tag{7a}$$

$$I_2 = k_{eff}(V_B - V_d - V_{T\Sigma})^2 \tag{7b}$$

Using current mirrors the differential output current

$$\begin{aligned} I_{out} &= I_1 - I_2 \\ &= 4k_{eff}(V_B - V_{T\Sigma})V_d \\ &= 4k_{eff}[\sqrt{(I_B/k_n)} - V_{Tp})V_d \end{aligned} \tag{8}$$